Precision timing of PSR J0437−4715: an accurate pulsar distance, a high pulsar mass and a limit on the variation of Newton's gravitational constant

J. P. W. Verbiest,[1,2] M. Bailes,[1] W. van Straten,[1] G. B. Hobbs,[2] R. T. Edwards,[2] R. N. Manchester,[2] N. D. R. Bhat,[1] J. M. Sarkissian,[2] B. A. Jacoby[3] and S. R. Kulkarni[4]

ABSTRACT

Analysis of ten years of high-precision timing data on the millisecond pulsar PSR J0437−4715 has resulted in a model-independent kinematic distance based on an apparent orbital period derivative, $\dot{P}_{\rm b}$, determined at the 1.5% level of precision ($D_{\rm k} = 157.0 \pm 2.4\,{\rm pc}$), making it one of the most accurate stellar distance estimates published to date. The discrepancy between this measurement and a previously published parallax distance estimate is attributed to errors in the DE200 Solar System ephemerides. The precise measurement of $\dot{P}_{\rm b}$ allows a limit on the variation of Newton's gravitational constant, $|\dot{G}/G| \leq 23 \times 10^{-12}\,{\rm yr}^{-1}$. We also constrain any anomalous acceleration along the line of sight to the pulsar to $|a_\odot/c| \leq 1.5 \times 10^{-18}\,{\rm s}^{-1}$ at 95% confidence, and derive a pulsar mass, $m_{\rm psr} = 1.76 \pm 0.20\,M_\odot$, one of the highest estimates so far obtained.

Subject headings: stars: distances — pulsars: individual (PSR J0437−4715) — stars: neutron

1. Introduction

In 1993, Johnston et al. reported the discovery of PSR J0437−4715, the nearest and brightest millisecond pulsar known. Within a year, the white dwarf companion and pulsar

[1]Centre for Astrophysics and Supercomputing, Swinburne Unversity of Technology, P.O. Box 218 Hawthorn, VIC 3122, Australia

[2]Australia Telescope National Facility – CSIRO, P.O. Box 76, Epping, NSW 1710, Australia

[3]Naval Research Laboratory, 4555 Overlook Avenue, SW, Washington, DC 20375

[4]Robinson Laboratory, California Institute of Technology, Mail Code 105-24, Caltech Optical Observatories, Pasadena, CA 91125

wind bow shock were observed (Bell, Bailes & Bessell 1993) and pulsed X-rays were detected (Becker & Trümper 1993). The proper motion and an initial estimate of the parallax were later presented along with evidence for secular change in the inclination angle of the orbit due to proper motion (Sandhu et al. 1997). Using high time resolution instrumentation, the three-dimensional orbital geometry of the binary system was determined, enabling a new test of general relativity (GR; van Straten et al. 2001). Most recently, multi-frequency observations were used to compute the dispersion measure structure function (You et al. 2007), quantifying the turbulent character of the interstellar medium towards this pulsar.

The high proper motion and proximity of PSR J0437−4715 led to the prediction (Bell & Bailes 1996) that a distance measurement independent of parallax would be available within a decade, when the orbital period derivative ($\dot{P}_{\rm b}$) would be determined to high accuracy. Even if the predicted precision of ∼1% would not be achieved, such a measurement would be significant given the strong dependence of most methods of distance determination on relatively poorly constrained models and the typically large errors on parallax measurements. Even for nearby stars, both the Hubble Space Telescope and the Hipparcos satellite give typical distance errors of 3% (Valls-Gabaud 2007) and so far only two distances beyond 100 pc have been determined at $\sim 1\%$ uncertainty (Torres et al. 2007). This kinematic distance is one of the few model-independent methods that does not rely upon the motion of the Earth around the Sun.

As demonstrated by Damour & Taylor (1991), $\dot{P}_{\rm b}$ can also be used to constrain the variation of Newton's gravitational constant. The best such limit from pulsar timing to date (Taylor 1993, $|\dot{G}/G| = (4 \pm 5) \times 10^{-12}\,{\rm yr}^{-1}$ from PSR B1913+16) is compromised due to the poorly constrained equation of state for the neutron star companion (Nordtvedt 1990). The slightly weaker but more reliable limit of $|\dot{G}/G| = (-9 \pm 18) \times 10^{-12}\,{\rm yr}^{-1}$ (Kaspi, Taylor & Ryba 1994, from PSR B1855+09, which has a white dwarf companion) should therefore be considered instead. A more stringent limit can be obtained from the Splaver et al. (2005) timing of PSR J1713+0747: $|\dot{G}/G| = (2.5 \pm 3.3) \times 10^{-12}\,yr^{-1}$ (at 95% certainty). This limit is, however, based upon the formal errors of $\dot{P}_{\rm b}$, $P_{\rm b}$ and parallax, which are easily underestimated by standard methodologies, as we shall demonstrate later. Because of this we believe the Splaver et al. (2005) limit is probably underestimated, but still of relevance. However, none of these limits are as strong as that put by lunar laser ranging (LLR; Williams, Turyshev & Boggs 2004): $\dot{G}/G = (4 \pm 9) \times 10^{-13}\,{\rm yr}^{-1}$. Besides limiting alternative theories of gravity, bounds on $\dot{G}$ can also be used to constrain variations of the Astronomical Unit (AU). Current planetary radar experiments (Krasinsky & Brumberg 2004) have measured a significant linear increase of $dAU/dt = 0.15 \pm 0.04\,{\rm m\ yr}^{-1}$, which may imply $\dot{G}/G = (-10 \pm 3) \times 10^{-13}\,{\rm yr}^{-1}$, just beyond the sensitivity of the limits listed above.

As mentioned before, the equation of state for dense neutron star matter is very poorly constrained. Pulsar mass determinations can probe the range of permissible pulsar masses and thereby limit possible equations of state (Lattimer & Prakash 2007). Presently, only the pulsars NGC 6440B, Terzan 5 I and Terzan 5 J have predicted masses higher than the typical value of $1.4\,M_{\odot}$(Freire et al. 2007; Ransom et al. 2005); however, as discussed in more detail in Section 5, such predictions do not represent objective mass estimates.

The remainder of this paper is structured as follows: Section 2 describes the observations, data analysis and general timing solution for PSR J0437−4715. Section 3 describes how the measurement of $\dot{P}_{\rm b}$ leads to a new and highly precise distance. In Section 4, this measurement is combined with the parallax distance to derive limits on $\dot{G}$ and the Solar System acceleration. Section 5 presents the newly revised pulsar mass and our conclusions are summarised in Section 6.

2. Observations and Data Reduction

Observations of PSR J0437−4715 were made over a time span of ten years (see Figure 1), using the Parkes 64-m radio telescope, two 20 cm receiving systems (the central beam of the Parkes multi-beam receiver (Staveley-Smith et al. 1996) and the H-OH receiver) and four generations of digital instrumentation (see Table 1): the Fast Pulsar Timing Machine (FPTM), the S2 VLBI recorder, and the Caltech-Parkes-Swinburne Recorders (CPSR and CPSR2). The FPTM is an autocorrelation spectrometer, whereas the three other instruments are baseband data recording and processing systems that employ phase-coherent dispersion removal.

2.1. Arrival Time Estimation

For the FPTM, S2, and CPSR backends, the uncalibrated polarization data were combined to form the polarimetric invariant interval (Britton 2000) and each observation was integrated in time and frequency before pulse arrival times were calculated through standard cross-correlation with an instrument-dependent template profile. For the CPSR2 data, the technique described by van Straten (2004) was used to calibrate 5 days of intensive PSR J0437−4715 observations made on 2003 July 19 to 21, 2003 August 29, and 2005 July 24. The calibrated data were integrated to form a polarimetric template profile with an integration length of approximately 40 hours and frequency resolution of 500 kHz. This template profile and Matrix Template Matching (MTM, van Straten 2006) were used to calibrate the

three years of CPSR2 data. An independent MTM fit was performed on each five-minute integration, producing a unique solution in each frequency channel, as shown in Figure 2 of van Straten (2006). The calibrated data were then integrated in frequency to produce a single full-polarization profile at each epoch. MTM was then used to derive time-of-arrival (TOA) estimates from each calibrated, five-minute integration. The application of MTM during the calibration and timing stages reduced the weighted rms of the CPSR2 post-fit timing residuals by a factor of two. All the data reduction described above was performed using the PSRCHIVE software package (Hotan, van Straten & Manchester 2004).

2.2. Timing Analysis

Most data were recorded at a wavelength of 20 cm; however, in the final three years, simultaneous observations at 10 and 50 cm were used to measure temporal variations of the interstellar dispersion delay (corrections for these variations were implemented in a way similar to that of You et al. 2007). A linear trend of these delays was also obtained for the year of FPTM data, using data at slightly different frequencies close to 1400 MHz.

The arrival times were analyzed using the TEMPO2 pulsar timing software package (Hobbs, Edwards & Manchester 2006; Edwards, Hobbs & Manchester 2006) and consistency with the earlier program, TEMPO, was verified. The timing model (see Table 2) is based on the relativistic binary model first derived by Damour & Deruelle (1986), and expanded to contain the geometric orbital terms described by Kopeikin (1995, 1996). The model is optimised through a standard weighted least-squares fit in which all parameters are allowed to vary, including the unknown time delays between data from different instruments, but excluding the mean value of dispersion measure, which is determined from the simultaneous CPSR2, 64 MHz-wide bands centred at 1341 and 1405 MHz.

A major difference between our implementation of solutions for the orbital angles Ω and i and previous efforts (van Straten et al. 2001; Hotan, Bailes & Ord 2006) is that they were implemented as part of the standard fitting routine. This ensures any covariances between these and other parameters (most importantly the periastron advance and companion mass, see Table 2 and Section 5) are properly accounted for, thereby yielding a more reliable measurement error. The previous works mentioned above derived these effects from an independent mapping of χ^2 space, leaving the errors of other parameters unaffected.

As can be seen from Figure 1, there are significant low-frequency structures present in the timing residual data. Since the standard least-squares fitting routine used in TEMPO2 does not account for the effect of such correlations on parameter estimation, we performed a

Monte-Carlo simulation where data sets with a post-fit power spectrum statistically consistent with that of the PSR J0437−4715 data were used to determine the parameter estimations uncertainties in the presence of realistic low frequency noise. These errors, as well as the factors by which the original errors were underestimated, are shown in Table 2. As an example, the distribution of derived pulsar masses from the Monte-Carlo simulation is given in Figure 2. Because of the dispersion measure corrections implemented in the final three years of data, one can expect the spectrum of these most precise data points to contain less low-frequency noise than the ten year data set as a whole. We therefore expect the errors resulting from this analysis to be slightly overestimated. Ongoing research into extending the fitting routine with reliable whitening schemes to avoid the spectral leakage and hence improve the reliability of the measured parameters, is expected to reduce these errors by factors of around two. All errors given in this paper are those resulting from the Monte-Carlo simulations, unless otherwise stated. The simulations also showed that any biases resulting from the red noise are statistically negligible for the reported parameters. (A full description of this Monte-Carlo technique and the whitening schemes mentioned will be detailed in a future publication.)

2.3. Solar System Ephemerides

Pulsar timing results are dependent on accurate ephemerides for the Solar System bodies. The results presented in this paper were obtained using the DE405 model (Standish 2004) and, for comparison, selected parameters obtained with the earlier DE200 model are shown in Table 3. The greatly reduced χ^2 indicates that the newer Solar System ephemerides are superior to the earlier DE200, reinforcing similar conclusions of other authors (Splaver et al. 2005; Hotan, Bailes & Ord 2006). We notice the parallax value changes by more than $10\,\sigma$, and that the different derived values are closely correlated with the ephemeris used. Although the effect is not as dramatic as it appears because of the under-estimation of the TEMPO2 errors, the fact that the DE405 results agree much better with the more accurate kinematic distance (discussed in the next Section), strongly suggests that the differences are due to the ephemeris used and confirms that the DE405 ephemeris is superior. Finally, we note that the DE405 measurement of $\dot{\omega}$ ($0.016 \pm 0.008\,^{\circ}\mathrm{yr}^{-1}$) is consistent with the GR prediction for this system ($0.0172 \pm 0.0009\,^{\circ}\mathrm{yr}^{-1}$).

3. Kinematic Distance

As shown in Figure 3, the long-term timing history enables precise measurement of the orbital period derivative, $\dot{P}_{\rm b}= (3.73 \pm 0.06) \times 10^{-12}$. This observed value represents a combination of phenomena that are intrinsic to the binary system and dynamical effects that result in both real and apparent accelerations of the binary system along the line of sight (Bell & Bailes 1996); i.e.

$$\dot{P}_{\rm b}^{\rm obs} = \dot{P}_{\rm b}^{\rm int} + \dot{P}_{\rm b}^{\rm Gal} + \dot{P}_{\rm b}^{\rm kin} \tag{1}$$

where "obs" and "int" refer to the observed and intrinsic values; "Gal" and "kin" are the Galactic and kinematic contributions.

Intrinsic orbital decay is a result of energy loss typically due to effects such as atmospheric drag and tidal dissipation; however, in a neutron star–white dwarf binary system like PSR J0437−4715, energy loss is dominated by quadrupolar gravitational wave emission. For this system, GR predicts (Taylor & Weisberg 1982) $\dot{P}_{\rm b}^{\rm GR} = -4.2 \times 10^{-16}$, two orders of magnitude smaller than the uncertainty in the measured value of $\dot{P}_{\rm b}$.

Galactic contributions to the observed orbital period derivative include differential rotation and gravitational acceleration (Damour & Taylor 1991). The differential rotation in the plane of the Galaxy is estimated from the Galactic longitude of the pulsar and the Galactocentric distance and circular velocity of the Sun. Acceleration in the Galactic gravitational potential varies as a function of height above the Galactic plane (Holmberg & Flynn 2004), which may be estimated using the parallax distance and the Galactic latitude of the pulsar. Combining these terms gives $\dot{P}_{\rm b}^{\rm Gal} = (-1.8 - 0.5) \times 10^{-14} = -2.3 \times 10^{-14}$, which is of the same order as the current measurement error.

Given the negligible intrinsic contribution, Equation 1 can be simplified and rewritten in terms of the dominant kinematic contribution known as the Shklovskii effect (Shklovskii 1970), an apparent acceleration resulting from the non-linear increase in radial distance as the pulsar moves across the plane perpendicular to the line of sight; quantified by the proper motion, μ, and distance D from the Earth:

$$\dot{P}_{\rm b}^{\rm obs} - \dot{P}_{\rm b}^{\rm Gal} \simeq \dot{P}_{\rm b}^{\rm kin} = \frac{\mu^2 D}{c} P_{\rm b}, \tag{2}$$

where c is the vacuum speed of light. Using the measured values of μ, $P_{\rm b}$, and $\dot{P}_{\rm b}$, Equation 2 is used to derive the kinematic distance (Bell & Bailes 1996): $D_k = 157.0 \pm 2.4$ pc. This distance is consistent with the one derived from parallax ($D_\pi = 150 \pm 12$ pc – see also Figure 4) and is, with a relative error of 1.5%, comparable in precision to the best parallax measurements from VLBI (Torres et al. 2007) and better than typical relative errors provided by the Hipparcos and Hubble space telescopes (Valls-Gabaud 2007).

Given the dependence of parallax distances on ephemerides, as described in Section 2.3, it is interesting to note the robustness of $D_{\rm k}$. Also, Table 2 shows that the presence of red noise corrupts the parallax error by a factor of 7.9, whereas $\dot{P}_{\rm b}$ is only affected by a factor of 2.5. These facts clearly indicate the higher reliability of $D_{\rm k}$ as compared to D_{π}.

4. Limits on $\dot{P}_{\rm b}$ Anomalies: $\dot{G}$ and the Acceleration of the Solar System

Any anomalous orbital period derivative can be constrained by substituting the parallax distance into Equation 2, yielding

$$\begin{aligned}\left(\frac{\dot{P}_{\rm b}}{P_{\rm b}}\right)^{\rm excess} &= (\dot{P}_{\rm b}^{\rm obs} - \dot{P}_{\rm b}^{\rm Gal} - \dot{P}_{\rm b}^{\rm kin})/P_{\rm b} \\ &= (3.2 \pm 5.7) \times 10^{-19}\,{\rm s}^{-1}. \end{aligned} \quad (3)$$

in which the error is almost exclusively due to the parallax uncertainty. Following Damour & Taylor (1991), this can be translated into a limit on the time derivative of Newton's gravitational constant (given are 95% confidence levels):

$$\frac{\dot{G}}{G} = -\frac{1}{2}\left(\frac{\dot{P}_{\rm b}}{P_{\rm b}}\right)^{\rm excess} = (-5 \pm 18) \times 10^{-12}\,{\rm yr}^{-1} \quad (4)$$

This limit is of the same order as those previously derived from pulsar timing (see Section 1), but a currently ongoing VLBI campaign on this pulsar is expected to improve significantly on our parallax measurement, and this should improve our limit to close to that put by LLR ($(4 \pm 9) \times 10^{-13}$ yr^{-1}; Williams, Turyshev & Boggs 2004). The LLR experiment is based on a complex n–body relativistic model of the planets that incorporates over 140 estimated parameters, such as elastic deformation, rotational dissipation and two tidal dissipation parameters. In contrast, the PSR J0437−4715 timing result is dependent on a different set of models and assumptions, and therefore provides a useful independent confirmation of the LLR result.

A recent investigation into the possible causes of a measured variability of the Astronomical Unit (AU; Krasinsky & Brumberg 2004) has refuted all but two sources of the measured value of $dAU/dt = 0.15 \pm 0.04$ m/yr. Krasinsky & Brumberg (2004) state that the measured linear increase in the AU would be due to either systematic effects or to a time-variation of G at the level of $\dot{G}/G = (-10 \pm 3) \times 10^{-13}\,{\rm yr}^{-1}$, comparable to, but inconsistent with, the LLR limit.

The anomalous $\dot{P}_{\rm b}$ measurements of a number of millisecond pulsars have also been used to place limits on the acceleration of the Solar System due to any nearby stars or undetected

massive planets (Zakamska & Tremaine 2005). The PSR J0437−4715 data set limits any anomalous Solar System acceleration to $|a_\odot/c| \leq 1.5 \times 10^{-18}\,\mathrm{s}^{-1}$ in the direction of the pulsar with 95% certainty. This rules out any Jupiter-mass planets at distances less than 117 AU along the line of sight, corresponding to orbital periods of up to 1270 years. Similarly, this analysis excludes any Jupiter-mass planets orbiting PSR J0437−4715 between ∼5 and 117 AU along the line of sight. Zakamska & Tremaine (2005) also compared the sensitivity of this limit to that of optical and infra-red searches for trans-Neptunian objects (TNOs) and concluded that beyond ∼ 300 AU the acceleration limit becomes more sensitive than the alternative searches. At a distance of 300 AU from the Sun, the 95% confidence upper limit on the mass of a possible TNO (in the direction of the pulsar) is 6.8 Jupiter masses. The precise VLBI measurement of parallax mentioned above might decrease this to close to one Jupiter mass.

5. Pulsar Mass

A combination of the mass function and a measurement of the Shapiro delay range can be used to obtain a measurement of the pulsar mass. Using this method, van Straten et al. (2001) derived a mass for PSR J0437−4715 of $1.58 \pm 0.18\,M_\odot$ whereas Hotan, Bailes & Ord (2006) obtained $1.3 \pm 0.2\,M_\odot$. It should be noted, however, that these values resulted from a model that incorporated geometric parameters first described by Kopeikin (1995, 1996), but covariances between these and other timing parameters (most importantly the companion mass or Shapiro delay range) were not taken into account. Whilst the length of the data sets used by these authors were only a few years, it can also be expected that some spectral leakage from low-frequency noise was unaccounted in the errors of these previously published values. As described in Section 2, the Monte-Carlo simulations and extended fitting routines implemented for the results reported in this paper do include these covariances and spectral leakage; it can therefore be claimed that the current estimates (at 68% confidence) of $m_\mathrm{c} = 0.254 \pm 0.018\,M_\odot$ and $m_\mathrm{psr} = 1.76 \pm 0.20\,M_\odot$, for the white dwarf companion and pulsar respectively, reflect the measurement uncertainty more realistically than any previous estimate. The distribution of m_psr that follows from the 5000 Monte-Carlo realizations is shown in Figure 2, together with a Gaussian with mean 1.76 and standard deviation 0.20. This demonstrates the symmetric distribution of the pulsar mass likelihood distribution, induced by the precise determination of the orbital inclination angle.

We also note that the new mass measurement of PSR J0437−4715 is the highest obtained for any pulsar to date. Distinction needs to be made between the objective mass estimate presented in this paper and the subjective mass predictions presented in Ransom et al.

(2005) and Freire et al. (2007). The pulsar mass confidence interval presented in this paper is derived from the measurement uncertainties of all relevant model parameters, including the well-determined orbital inclination angle, i. In contrast, i is unknown in the Terzan 5 I and J (Ransom et al. 2005) and PSR J1748−2021B (Freire et al. 2007) binary systems, and the posterior probability intervals for the pulsar masses presented in these works are based upon the prior assumption of a uniform distribution of $\cos i$. These fundamental differences must be accounted for in any subsequent hypothesis testing. Consequently, PSR J0437−4715 is currently the only pulsar to provide reliable constraints on equations of state based on hyperons and Bose-Einstein condensates as described by Lattimer & Prakash (2007). Simulations with TEMPO2 indicate that a forthcoming observational campaign with a new generation of backend systems can be expected to increase the significance of this measurement by another factor of about two in the next year.

6. Conclusions

We have presented results from the highest-precision long-term timing campaign to date. With an overall residual rms of 199 ns, the 10 years of timing data on PSR J0437−4715 have provided a precise measurement of the orbital period derivative, $\dot{P}_{\rm b}$, leading to the first accurate kinematic distance to a millisecond pulsar: $D_{\rm k} = 157.0 \pm 2.4\,{\rm pc}$. Application of this method to other pulsars in the future can be expected to improve distance estimates to other binary pulsar systems (Bell & Bailes 1996).

Another analysis based on the $\dot{P}_{\rm b}$ measurement places a limit on the temporal variation of Newton's gravitational constant. We find a bound comparable to the best so far derived from pulsar timing: $\dot{G}/G = (-5 \pm 18) \times 10^{-12}\,{\rm yr}^{-1}$. An ongoing VLBI campaign on this pulsar is expected to improve this limit, enabling an independent confirmation of the LLR limit.

Previous estimates of the mass of PSR J0437−4715 have been revised upwards to $m_{\rm psr} = 1.76 \pm 0.20\,M_\odot$, which now makes it one of the few pulsars with such a heavy mass measurement. A new generation of backend instruments, dedicated observing campaigns, and data prewhitening techniques currently under development should decrease the error in this measurement enough to significantly rule out various equations of state for dense nuclear matter.

The Parkes Observatory is part of the Australia Telescope which is funded by the Commonwealth of Australia for operation as a National Facility managed by CSIRO. We thank the staff at Parkes Observatory for technical assistance during regular observations. B.A.J

holds a National Research Council Research Associateship Award at the Naval Research Laboratory (NRL). Basic research in radio astronomy at NRL is supported by the Office of Naval Research. The authors wish to express their gratitude to William Coles from the University of California at San Diego, for extensive discussion and help with the Monte-Carlo error analysis. Finally, we thank the referee for valuable and inspiring comments.

Facilities: Parkes

REFERENCES

Becker, W. and Trümper, J. 1993, Nature, 365, 528.

Bell, J. F. and Bailes, M. 1996, ApJ, 456, L33.

Bell, J. F., Bailes, M., and Bessell, M. S. 1993, Nature, 364, 603.

Britton, M. C. 2000, ApJ, 532, 1240.

Damour, T. and Deruelle, N. 1986, Ann. Inst. H. Poincaré (Physique Théorique), 44, 263.

Damour, T. and Taylor, J. H. 1991, ApJ, 366, 501.

Edwards, R. T., Hobbs, G. B., and Manchester, R. N. 2006, MNRAS, 372, 1549.

Foster, R. S. and Backer, D. C. 1990, ApJ, 361, 300.

Freire, P. C. C., Ransom, S. M., Begin, S., Stairs, I. H., Hessels, J. W. T., Frey, L. H., and Camilo, F. 2007, ArXiv e-prints, 0711.0925.

Hobbs, G. 2005, Proc. Astron. Soc. Austral., 22, 179.

Hobbs, G. B., Edwards, R. T., and Manchester, R. N. 2006, MNRAS, 369, 655.

Holmberg, J. and Flynn, C. 2004, MNRAS, 352, 440.

Hotan, A. W., Bailes, M., and Ord, S. M. 2006, MNRAS, 369, 1502.

Hotan, A. W., van Straten, W., and Manchester, R. N. 2004, Proc. Astron. Soc. Austral., 21, 302.

Jenet, F. A. et al. 2006, ApJ, 653, 1571.

Johnston, S. et al. 1993, Nature, 361, 613.

Kaspi, V. M., Taylor, J. H., and Ryba, M. 1994, ApJ, 428, 713.

Kopeikin, S. M. 1995, ApJ, 439, L5.

Kopeikin, S. M. 1996, ApJ, 467, L93.

Krasinsky, G. A. and Brumberg, V. A. 2004, Celestial Mechanics and Dynamical Astronomy, 90, 267.

Lattimer, J. M. and Prakash, M. 2007, Phys. Rep., 442, 109.

Nordtvedt, K. 1990, Phys. Rev. Letters, 65, 953.

Ransom, S. M., Hessels, J. W. T., Stairs, I. H., Freire, P. C. C., Camilo, F., Kaspi, V. M., and Kaplan, D. L. 2005, Science, 307, 892.

Sandhu, J. S. 2001. PhD thesis, California Institute of Technology.

Sandhu, J. S., Bailes, M., Manchester, R. N., Navarro, J., Kulkarni, S. R., and Anderson, S. B. 1997, ApJ, 478, L95.

Shklovskii, I. S. 1970, Soviet Astron. AJ, 13, 562.

Splaver, E. M., Nice, D. J., Stairs, I. H., Lommen, A. N., and Backer, D. C. 2005, ApJ, 620, 405.

Standish, E. M. 2004, A&A, 417, 1165.

Staveley-Smith, L. et al. 1996, Publications of the Astronomical Society of Australia, 13, 243.

Stinebring, D. R., Ryba, M. F., Taylor, J. H., and Romani, R. W. 1990, Phys. Rev. Letters, 65, 285.

Taylor, J. H. 1993, in Particle Astrophysics, ed. G. Fontaine and J. Tran Thanh van, 367.

Taylor, J. H. and Weisberg, J. M. 1982, ApJ, 253, 908.

Thorsett, S. E. and Chakrabarty, D. 1999, ApJ, 512, 288.

Torres, R. M., Loinard, L., Mioduszewski, A. J., and Rodriguez, L. F. 2007, ArXiv e-prints, 708.

Valls-Gabaud, D. 2007, in IAU Symposium, volume 240 of IAU Symposium, 281.

van Straten, W. 2003. PhD thesis, Swinburne University of Technology.

van Straten, W. 2004, ApJS, 152, 129.

van Straten, W. 2006, ApJ, 642, 1004.

van Straten, W., Bailes, M., Britton, M., Kulkarni, S. R., Anderson, S. B., Manchester, R. N., and Sarkissian, J. 2001, Nature, 412, 158.

Williams, J. G., Turyshev, S. G., and Boggs, D. H. 2004, Phys. Rev. Letters, 93(26), 261101.

You, X.-P. et al. 2007, MNRAS, 378, 492.

Zakamska, N. L. and Tremaine, S. 2005, AJ, 130, 1939.

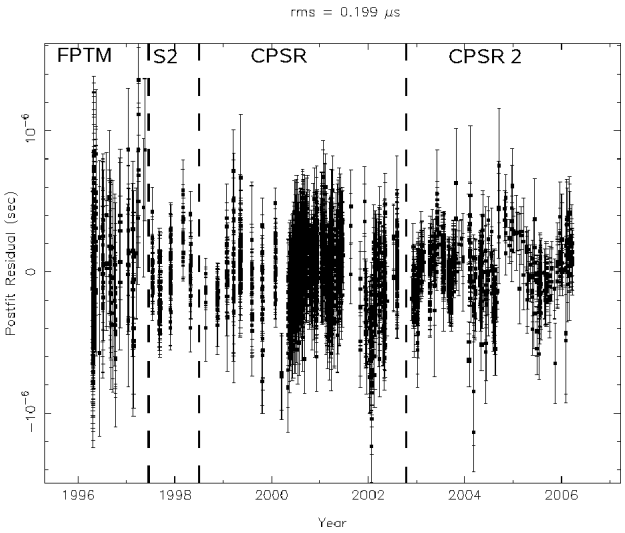

Fig. 1.— Combined 20 cm post-fit timing residuals for new and archival PSR J0437−4715 timing data. Vertical dashed lines separate the different instruments.

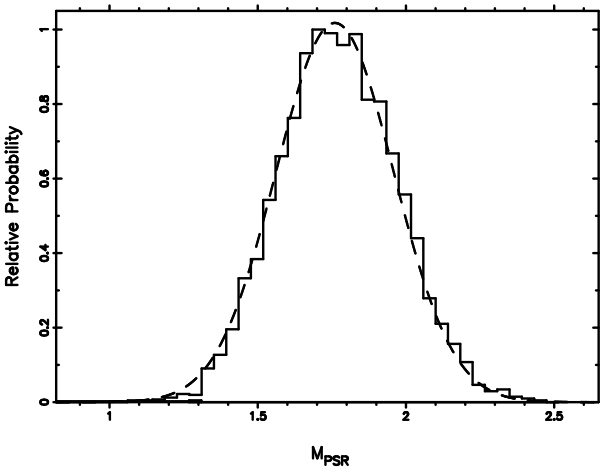

Fig. 2.— Pulsar mass probability distribution. The solid line shows the histogram of 5000 pulsar masses derived from a Monte-Carlo simulation with power spectrum and sampling equal to that of the PSR J0437−4715 data set. The dashed line is a Gaussian distribution with a mean value of $m_{\rm psr} = 1.76\,M_\odot$ and standard deviation of $0.20\,M_\odot$.

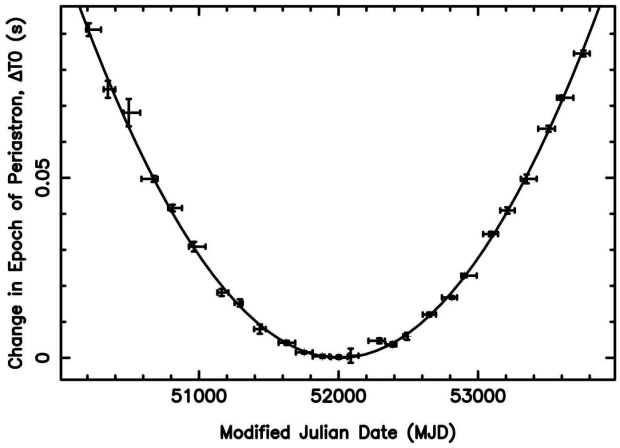

Fig. 3.— Variations in epoch of periastron passage (T_0) due to apparent orbital period increase. A steady increase in orbital period is equivalent to a quadratic increase in T_0 relative to periastron times for a constant orbital period. For this plot, T_0 was measured on data spans of up to 120 days with a model having no orbital period derivative. The formal one-σ measurement errors reported by TEMPO2 are shown by vertical error bars and the epochs over which the measurements were made are shown by horizontal bars. As the mean measurement time was determined through a weighted average of the data contained in the fit, these horizontal bars need not be centred at the mid time associated with the measurement. The parabola shows the effect of the $\dot{P}_{\rm b}$ value obtained from a fit to the data shown in Figure 1.

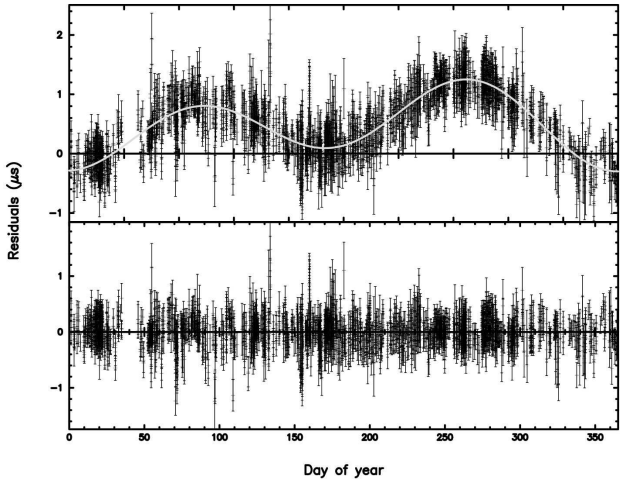

Fig. 4.— Parallax signature of PSR J0437−4715. Top: Timing residuals for PSR J0437−4715 as a function of day of year (starting on 18 November), without parallax but with all remaining parameters at their best-fit values. The smooth curve represents the model fit of a parallax of 6.65 mas. Bottom: The same timing residuals with parallax included in the model. The overall rms for the top and bottom plots is 524 and 199 ns respectively. The double-humped signature specific to parallax originates from the delay in pulse time-of-arrival (TOA) as the Earth orbits the Sun and samples different parts of the curved wave-front originating at the pulsar.

Table 1. Characteristics of the timing data for the four instruments used

Backend	Date range	Ref.	Bandwidth	RMS Residual	Observation length[a]	Number of TOAs	TOA error[a]
FPTM	1996 Apr – 1997 May	1,2	256 MHz	368 ns	10 min	207	500 ns
S2	1997 Jul – 1998 Apr	3	16 MHz	210 ns	120 min	117	160 ns
CPSR	1998 Aug – 2002 Aug	3	20 MHz	218 ns	15 min	1782	250 ns
CPSR2	2002 Nov – 2006 Mar	4	2×64 MHz[b]	164 ns	60 min	741	150 ns

[a]Displayed are typical values only.

[b]CPSR2 records two adjacent 64 MHz bands simultaneously at 20 cm.

References. — (1) Sandhu et al. (1997); (2) Sandhu (2001); (3) van Straten (2003); (4) Hotan, Bailes & Ord (2006).

Table 2. PSR J0437−4715 timing model parameters[a]

Parameter Name and Units	Parameter Value	TEMPO2 Error[b]	Monte-Carlo Error[b]	Error Ratio
Fit and Data Set				
MJD range	50191.0–53819.2			
Number of TOAs	2847			
Rms timing residual (μs)	0.199			
Measured Quantities				
Right ascension, α (J2000)	$04^{\rm h}37^{\rm m}15\overset{\rm s}{.}8147635$	3	29	9.8
Declination, δ (J2000)	$-47°15'08\overset{''}{.}624170$	3	34	11
Proper motion in α, $\mu_\alpha \cos\delta$ (mas yr^{-1})	121.453	1	10	8.7
Proper motion in δ, μ_δ (mas yr^{-1})	−71.457	1	12	9.0
Annual parallax, π (mas)	6.65	7	51	7.9
Dispersion measure, DM (cm^{-3} pc)	2.64476	7	[d]	[d]
Pulse period, P (ms)	5.757451924362137	2	99	47
Pulse period derivative, $\dot{P}$ (10^{-20})	5.729370	2	9	4.8
Orbital period, $P_{\rm b}$ (days)	5.74104646[c]	108	200	1.9
Orbital period derivative, $\dot{P}_{\rm b}$ (10^{-12})	3.73	2	6	2.5
Epoch of periastron passage, T_0 (MJD)	52009.852429[c]	582	780	1.3
Projected semi-major axis, x (s)	3.36669708[c]	11	14	1.4
Longitude of periastron, ω_0 (°)	1.2224[c]	365	490	1.3
Orbital eccentricity, e (10^{-5})	1.9180	3	7	2.1
Periastron advance, $\dot{\omega}$ (° yr^{-1})	0.01600[c]	430	800	1.8
Companion mass, m_2 ($M_\odot$)	0.254[c]	14	18	1.3
Longitude of ascension, Ω (°)	207.8[c]	23	69	3.0
Orbital inclination, i (°)	137.58	6	21	3.7
Set Quantities				

Table 2—Continued

Parameter Name and Units	Parameter Value	TEMPO2 Error[b]	Monte-Carlo Error[b]	Error Ratio
Reference epoch for P, α and δ determination (MJD)	52005			
Reference epoch for DM determination (MJD)	53211			

[a]These parameters are determined using TEMPO2 which uses the International Celestial Reference System and Barycentric Coordinate Time. As a result this timing model must be modified before being used with an observing system that inputs TEMPO format parameters. See Hobbs, Edwards & Manchester (2006) for more information.

[b]Given uncertainties are 1σ values in the last digits of the parameter values.

[c]Because of large covariances, extra precision is given for selected parameters.

[d]Dispersion measure was determined through alignment of simultaneous CPSR2 observations centred at 1341 MHz and 1405 MHz. The effect of red noise is therefore not applicable.

Table 3. Comparison of DE200 and DE405 results for PSR J0437−4715[a]

Parameter name	DE200 result	DE405 result
Rms residual (ns)	281	199
Relative χ^2	2.01	1.0
Parallax, π (mas)	7.84(7)	6.65 (7)
Parallax distance, D_π (pc)	127.6(11)	150.4(16)
Previously published π (mas)	7.19(14)[1]	6.3(2)[2]
Kinematic distance, D_k (pc)	154.5 (10)	156.0 (10)
D_k corrected for Galactic effects (pc)	155.5 (10)	157.0 (10)
Variation of Newton's gravitational constant, $\lvert\dot{G}/G\rvert$ (10^{-12} yr^{-1}).....	−21.2(22)[b]	−5.0(26)[b]
Total proper motion, μ_{tot} (mas yr^{-1})	140.852(1)	140.915(1)
Companion mass, m_c ($M_\odot$)	0.263(14)	0.254(14)
Pulsar mass, m_{psr} ($M_\odot$)	1.85(15)	1.76(15)
Periastron advance, $\dot{\omega}$ ($^\circ$ yr^{-1})	0.020(4)	0.016(4)
GR prediction of $\dot{\omega}$ ($^\circ$ yr^{-1})	0.0178(9)	0.0172(9)

[a]Numbers in parentheses represent the formal TEMPO2 1 σ uncertainty in the last digits quoted, unless otherwise stated.

[b]Given are 2 σ errors, i.e. 95% confidence levels.

References. — (1) van Straten et al. (2001); (2) Hotan, Bailes & Ord (2006)